Predicted Permeability of the Cornea to Topical Drugs

Aurélie Edwards[1,3] and Mark R. Prausnitz[2]

Received July 25, 2001; accepted August 3, 2001

Purpose. To develop a theoretical model to predict the passive, steady-state permeability of cornea and its component layers (epithelium, stroma, and endothelium) as a function of drug size and distribution coefficient (Φ). The parameters of the model should represent physical properties that can be independently estimated and have physically interpretable meaning.

Methods. A model was developed to predict corneal permeability using 1) a newly developed composite porous-medium approach to model transport through the transcellular and paracellular pathways across the epithelium and endothelium and 2) previous work on modeling corneal stroma using a fiber-matrix approach.

Results. The model, which predicts corneal permeability for molecules having a broad range of size and lipophilicity, was validated by comparison with over 150 different experimental data points and showed agreement with a mean absolute fractional error of 2.43, which is within the confidence interval of the data. In addition to overall corneal permeability, the model permitted independent analysis of transcellular and paracellular pathways in epithelium, stroma and endothelium. This yielded strategies to enhance corneal permeability by targeting epithelial paracellular pathways for hydrophilic compounds ($\Phi < 0.1 - 1$), epithelial transcellular pathways for intermediate compounds, and stromal pathways for hydrophobic compounds ($\Phi > 10 - 100$). The effects of changing corneal physical properties (e.g., to mimic disease states or animals models) were also examined.

Conclusions. A model based on physicochemical properties of the cornea and drug molecules can be broadly applied to predict corneal permeability and suggest strategies to enhance that permeability.

KEY WORDS: ophthalmic drug delivery; theoretical model; eye; ophthalmology; ocular transport prediction.

INTRODUCTION

Topical drug delivery to the eye is the most common treatment of ophthalmic diseases, and the cornea provides the dominant barrier to drug transport (1). For this reason, a large body of experimental work has characterized corneal permeability (2), and some models have been developed as a result to describe transcorneal transport (3–7). However, most existing models rely on parameters that are fitted to a small number of experimental measurements and are not applicable to larger data sets, and many models do not account for all existing transport processes and routes. A model that can predict the corneal permeability of any drug based on its physical properties and those of the cornea would be more broadly useful.

If all the variables of a predictive model correspond to physical properties that are independently measured (such as molecular radius, width of intercellular spaces, etc.), the model then should not only describe the data used in its development but also predict corneal permeability to classes of compounds not considered during model development. With such a tool, the ability to deliver newly synthesized or even computer-generated drugs can be assessed without stepping into the laboratory. In addition, transport processes can be understood in physical terms (e.g., epithelial tight junctions are the rate-limiting barrier for a given drug), which helps develop appropriate ways to enhance or target delivery and facilitates predicting or analyzing delivery problems. Finally, because model variables have physical meaning, they can be easily changed to reflect the properties of diseased or injured cornea and to account for differences between humans and animals.

Given the potential power of an approach based on physics rather than statistics, we developed a model that builds off of previous work describing the permeability of corneal stroma (and sclera) by modeling it as a fiber matrix (8) and combines it with a new analysis presented for the corneal epithelium and endothelium. Both transcellular and paracellular transport pathways were considered and, whenever possible, parameters were derived from independent experimental observations.

MODEL DEVELOPMENT

Following the general approach taken by a number of previous studies (4,6,9), the steady-state permeability of cornea can be determined by considering the individual permeabilities of the three primary tissues that make up cornea: endothelium, stroma, and epithelium (10). Because Bowmann's membrane and Descemet's membranes are so thin and permeable, they do not contribute significantly to overall corneal permeability and are therefore not considered in this analysis. We have developed previously a model that predicts the permeability of stroma and that of the paracellular pathway across endothelium (8). In this section, we summarize these findings and develop new expressions for transport across the epithelium and the transcellular pathway across endothelium.

Endothelium

The corneal endothelium is a monolayer of hexagonal cells, each about 20 μm wide and 5 μm thick, found at the internal base of the cornea (10). Two pathways are available for solutes diffusing across the endothelium (Fig. 1): a paracellular route (i.e., between cells), which is a water-filled pathway impeded by gap and tight junctions and is favored by hydrophilic molecules and ions; and a transcellular route (i.e., within or across cell membranes), which involves partitioning into and diffusing within cell membranes and is the pathway of choice for hydrophobic molecules. The fraction of a given solute that goes through each route is determined primarily by its membrane-to-water distribution coefficient (Φ). The larger Φ (i.e., for hydrophobic molecules), the greater the

[1] Department of Chemical and Biological Engineering, Tufts University, 4 Colby Street, Medford, Massachusetts 02155.

[2] Schools of Chemical and Biomedical Engineering, Georgia Institute of Technology, Atlanta, Georgia 30332–0100.

[3] To whom correspondence should be addressed. (e-mail: aurelie.edwards@tufts.edu)

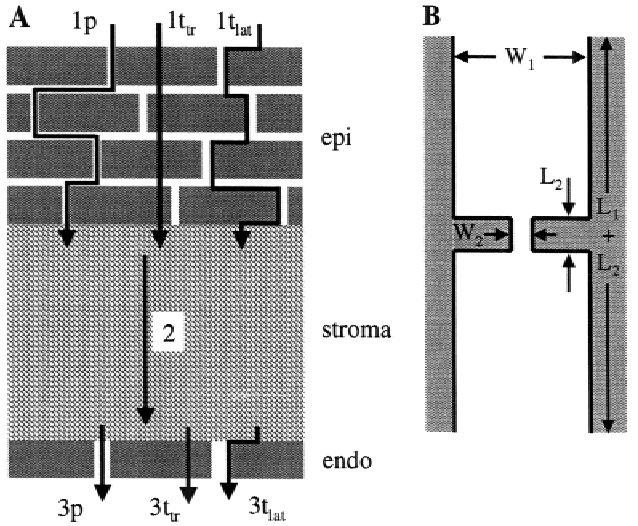

Fig. 1. An idealized representation of the cornea showing transport pathways across the epithelium, stroma, and endothelium (drawing not to scale). (A) In the epithelium, paracellular pathways follow the hydrophilic spaces between epithelial cells (1p), and transcellular pathways are either solely within the hydrophobic cell membranes ($1t_{lat}$) or alternate crossing of cell membranes and cell cytosol ($1t_{tr}$). The largely cell-free stroma offers only hydrophilic pathways among and between collagen fibers and proteoglycan matrix (2). The endothelium contains both hydrophilic paracellular (3p) and hydrophobic transcellular ($3t_{lat}$ and $3t_{tr}$) routes. (B) The paracellular spaces in epithelium and endothelium are modeled as slits with constrictions that represent tight and gap junctions.

relative amount of solute that diffuses through the cells. Because the two pathways are in parallel, the overall permeability of the cell layer (k_{layer}) is the sum of the permeabilities of each pathway:

$$k_{layer} = k_t + k_p \tag{1}$$

where k_t and k_p are the permeabilities of transcellular and paracellular routes, respectively. How to calculate the permeability of each of these pathways is described below.

Transcellular Pathway

The transcellular pathway across endothelium involves two possible routes. The first route consists of 1) partitioning from the water-rich stroma into the lipid-rich plasma membranes of endothelial cells; 2) diffusing within the cell membranes across the endothelium; and 3) partitioning out of the membranes and into the aqueous humor bathing the internal surface of the cornea. This pathway, referred to as the lateral route of the transcellular pathway (pathway $3t_{lat}$ in Fig. 1A), does not include transport within the cytosol of endothelial cells. The second route involves the following: 1) partitioning into, diffusing transversely across, and partitioning out of the anterior cell membrane; 2) diffusing through the cytosol; and 3) partitioning into, diffusing across, and partitioning out of the posterior cell membrane. This second pathway is referred to as the transverse route (pathway $3t_{tr}$ in Fig. 1A).

For simplicity, we assume those two routes can be treated separately. In reality, they are not independent: a molecule may follow a path involving a combination of lateral transport along the membrane and diffusion in the cytosol. Given this, the overall permeability of the transcellular route can be expressed as:

$$k_t = k_{lat} + k_{tr} \tag{2}$$

where k_{lat} and k_{tr} are the permeabilities of the lateral and transverse routes, respectively.

Lateral Diffusion. The permeability k_{lat} of the lateral transcellular pathway to a given solute is given by:

$$k_{lat} = \frac{\Phi D_{lat}}{L_{lat}} \tag{3}$$

where D_{lat} is the lateral diffusivity of the solute in the cell membranes and L_{lat} is the mean diffusion pathway length.

Our estimate of the lateral diffusivity of a small solute (~5 Å in radius) in the cell membranes of the cornea is 2×10^{-8} cm^2/s, based upon a compilation of experimental measurements reported by Johnson *et al.* (11), which were conducted using model cholesterol-containing lipid bilayers. This value is consistent with membrane diffusion studies in epithelial tissues (12). The mean diffusion pathway length, L_{lat}, was calculated as described below (Eq. 12). The average length of the paracellular opening between adjacent endothelial cells is L = 12.2 μm (13), and the average radius of an endothelial cell is 10 μm, yielding L_{lat} = 12.2 + 10/3 = 15.5 μm.

An empirical relationship between the membrane-to-water distribution coefficient and that between octanol and water (K_{ow}) is given by Johnson (Mark Johnson, personal communication):

$$\Phi = K_{ow}^{0.87} \tag{4}$$

The octanol-to-water distribution coefficient was determined using experimental values for the octanol-to-water partition coefficient and calculated values of the degree of solute ionization (assuming ionized molecules do not partition into octanol), as described and tabulated in Prausnitz and Noonan (2).

Transverse Diffusion. The permeability of the transverse route, k_{tr}, was calculated by considering three steps in series: transport across the anterior endothelial cell membrane, diffusion through cell cytoplasm, and transport across the posterior cell membrane.

$$\frac{1}{k_{tr}} = \frac{1}{k_{mem}} + \frac{1}{k_{cyt}} + \frac{1}{k_{mem}} = \frac{2}{k_{mem}} + \frac{1}{k_{cyt}} \tag{5}$$

where k_{mem} is cell membrane permeability and k_{cyt} is transcytosol permeability.

Endothelial cell membrane permeability was difficult to calculate because very few independent data are available. Most membrane permeability studies have used artificial lipid bilayers, which are more permeable than cell membranes. Lacking data on endothelial cell membrane permeability, we chose red blood cell (RBC) membranes as a model, which is the only cell membrane for which we could find useful data on transmembrane transport by passive mechanisms (i.e., diffusion).

Reliable measurements of RBC basal permeability have been compiled by Lieb and Stein (14). The octanol-to-water partition coefficient of the solutes considered in that study varies over a broad range between 1.2×10^{-3} and 1.1×10^{2}, but their molecular volume does not exceed 73 cm^3/mol (i.e., ~3 Å radius), meaning that data extrapolation was needed to include molecules typically delivered to the eye (i.e., radius of 3.5 to 5.5 Å). Recognizing this limitation, we used the model of Lieb and Stein for non-Stokesian diffusion (14), whereby the permeability of a cell membrane can be written as

$$k_{mem} = k^0_{mem}\, 10^{-m_v V} \tag{6}$$

where k^0_{mem} is the membrane permeability for a theoretical molecule of infinitely small size and the term $10^{-m_v V}$ accounts for the effects of molecular size; m_v is a measure of the size selectivity for diffusion within the membrane, which is 0.0516 mol/cm^3 for human RBCs (14), and V is the van der Waals molecular volume determined from molecular structure (2). The term K^0_{mem} has been empirically shown to depend on partition coefficient according to the following relationship.

$$\log(k^0_{mem}) = A \log(K_{ow}) + B \tag{7}$$

where k^0_{mem} has units of cm/s. Using octanol as a model for partitioning and assuming that the values of the distribution and partition coefficients are similar for the solutes being considered, the best-fit values of A and B were found to be 1.323 and –0.834, respectively, by linear regression of the RBC permeability data presented by Lieb and Stein (14).

Once the solute has crossed the cell membrane, it will diffuse within the cell cytoplasm. Cytosol-to-water diffusivity ratios have been found to be on the order of 1/4 (15), and we assumed that the average distance traveled within the cytosol from one side of the cell to the other is about $l_{cyt} = 5$ μm. The transcytosol permeability can thus be estimated as follows:

$$k_{cyt} = \frac{D_\infty}{4 l_{cyt}} \tag{8}$$

where D_∞ is the solute diffusivity in dilute bulk solution. Implicit in the equation given above is the assumption that solubility within the cytoplasm is equal to that within water.

Equation 6 yields transverse permeability values that are very low and almost always negligible compared to lateral permeability values. Because the data of Lieb and Stein (14) were obtained for molecular radii smaller than about 3 Å, it is possible that the expression accounting for the size dependence of k_{mem} does not apply to the larger solutes examined in this study. If Equation 6 overpredicts permeability (i.e., the actual transverse permeability is lower), overall model predictions would remain unchanged, because the transverse route would remain negligible. In contrast, underprediction could be problematic because transverse permeabilities could become significant and thereby increase corneal permeability predictions.

To assess the likelihood of over- or underprediction for larger molecules, we found literature values for transverse permeability across synthetic lipid bilayers for tryptophan ($K_{ow} = 9.1 \times 10^{-2}$) and citric acid ($K_{ow} = 1.9 \times 10^{-2}$), both of which have a radius of about 3.5 Å (16,17). These permeabilities have been measured as 4.1×10^{-10} and 3.1×10^{-11} cm/s, respectively, whereas Equation 6 predicts values of 1.6×10^{-8} and 2.1×10^{-9} cm/s, respectively. Although this large overprediction reduces our confidence in extrapolated predictions using Equation 6, it supports our overall conclusion that the transverse route is almost always negligible, because these measured permeabilities are even smaller than predicted.

Paracellular Pathway

Solutes that do not partition extensively into endothelial cell membranes and thus cannot access the transcellular pathway follow the paracellular route between the cells. As described by Fischbarg (13), the intercellular space between two endothelial cells can be idealized as a slit channel consisting of a wide section and a narrow one, the latter corresponding to the gap junction (Fig. 1B). The half-width of the wide part (W_1) and that of the narrow part (W_2) have been measured as 15 nm and 1.5 nm, respectively. The length of the wide part (L_1) has been determined to be 12 μm and that of the gap junction (L_2) is 0.24 μm (13).

Based on the theoretical results of Panwar and Anderson (18), the permeability k_i of a parallel-wall channel of half-width W_i and length L_i is given by:

$$k_i = \frac{f_i D_\infty}{L_i}\left[1 + \frac{9}{16}\left(\frac{r_s}{W_i}\right)\ln\left(\frac{r_s}{W_i}\right) - 1.19358\left(\frac{r_s}{W_i}\right) + 0.159317\left(\frac{r_s}{W_i}\right)^3\right] \tag{9}$$

where f_i is the fractional area of intercellular openings on the surface (i.e., porosity), and r_s is the solute radius. The total cell perimeter length per unit area is $l_c = 1200$ cm/cm^2 of endothelial surface (13), and f_i is estimated as $W_i \cdot l_c$. The term within brackets in Equation 9 represents the channel-to-free solution diffusivity ratio (including the effects of partitioning). D_∞ is determined using the Wilke-Chang equation (19) (for the molecules examined in this study, D_∞ is between 0.5×10^{-5} and 2×10^{-5} cm^2/s). Electrostatic effects are neglected in this approach, as suggested by previous studies (20). Also, note that because of tortuosity, the total length of the intercellular channel, $L_1 + L_2 = 12.2$ μm, is significantly greater than the cell thickness, which is equal to 5 μm.

The overall permeability of the paracellular pathway, consisting of the wide and narrow slit channels in series, is then given by:

$$k_p = \frac{1}{1/k_1 + 1/k_2} \tag{10}$$

Stroma

The stroma is a fibrous tissue that forms the bulk of the cornea and is made up primarily of large collagen fibers embedded in a proteoglycan matrix. We previously developed a model for the permeability of the stroma to small solutes and macromolecules (8). The analysis was performed on three length scales; for each, we assumed a given arrangement of fibers of defined geometry and orientation, around and through which solutes diffuse. Corresponding calculations were based on a fiber matrix approach. At the macroscale, stromal collagen lamellae are arranged in parallel sheets. At the mesoscale, the lamellae contain collagen fibrils forming hexagonal arrays of parallel cylinders. At the microscale, ground substance that surrounds the fibrils and lamellae was modeled as a randomly oriented collection of fibers, repre-

senting the proteoglycans. The corresponding equations are detailed in Edwards and Prausnitz (8) and are briefly summarized in the Appendix. It should be noted that in the previous study (8), a stromal hydration of 86% was used because we considered transport across isolated stroma, which has an increased water content. For this study, stromal hydration was taken as 78%, which is the physiologic value for intact cornea (8,10).

Epithelium

The epithelium is a multi-layer of cells found at the external surface of the cornea. The basal layer, separated from the stroma by a thin basement membrane, consists of a single sheet of columnar cells, about 20 μm high and 10 μm wide (10). Two or three layers of wing cells cover the basal cells, from which they are derived. As wing cells migrate towards the corneal surface, they flatten and give rise to two or three sheets of squamous cells that are about 4 μm thick and 20–45 μm wide. The total thickness of corneal epithelium is approximately 50–60 μm in humans (10). Similar to endothelium, the epithelium has two parallel pathways, a transcellular and a paracellular one (Fig. 1), meaning that Eq. 1 can be used.

Transcellular Pathway

The permeability of the transcellular pathway in the epithelium was calculated using Eq. 2; the values for k_{lat} and k_{tr} were determined as follows.

Lateral Diffusion. The permeability of the lateral route in the epithelium was calculated using Eq. 3, assuming that the only significant difference between lateral diffusion across corneal epithelium and endothelium is the pathway length, L_{lat}. That is, Φ and D_{lat} have the same values as in endothelium. We assumed that epithelial cells are packed very tightly so that there is almost no discontinuity as a solute diffuses from one cell to the other, i.e., membrane-to-membrane partitioning is not a rate-limiting step.

The mean diffusion pathway length, L_{lat}, was calculated assuming the cells are shaped like cylinders. Once a molecule partitions into a cell membrane somewhere on its upper surface, it must first diffuse across to the edge of the upper surface and then down along the side of the cell. The average distance $\langle r_i \rangle$ a molecule must diffuse across the upper circular surface of a cell i is equal to:

$$\langle r_i \rangle = R_i - \frac{1}{\pi R_i^2} \int_{r=0}^{R_i} \int_{\theta=0}^{2\pi} r^2 dr d\theta = \frac{R_i}{3} \qquad (11)$$

where R_i is the cell radius.

Assuming that the cells do not form columns but are randomly aligned, the mean pathway length is then given by:

$$L_{lat} = \sum_i \left(L_i + \frac{R_i}{3} \right) = L + \frac{1}{3} \sum_i R_i \qquad (12)$$

where L_i is the distance that a molecule must diffuse down along the side of a cell and L is the total diffusion length along the side of the cells, which is greater than the thickness of the epithelium because of tortuosity. In the 5-μm-thick endothelium, L has been measured as approximately 12 μm, i.e., a tortuosity of 2.4 (13). In the absence of data for the epithelium, we assumed that the tortuosity factor was the same in both barriers, and L was taken as 120 μm for the 50-μm-thick epithelium. In addition, we assumed an idealized epithelial geometry having three layers of squamous cells with a mean surface radius of 20 μm, three layers of wing cells of mean radius 10 μm, and one layer of columnar cells, 5 μm in radius (10). This yields $L_{lat} = 120 + 95/3 = 151.7$ μm.

Transverse Diffusion. To determine the permeability of the transverse route across epithelium, the permeability of a single cell membrane and that of the cytosol in a single cell were taken to be the same as in endothelium. Because epithelial cell layers can be represented as resistances in series, l_{cyt} was set equal to epithelium thickness, 50 μm, and Eq. 8 was used to calculate cytosol permeability. The permeability of a single cell membrane was determined using Eq. 6, and Eq. 5 was used to calculate permeability of the transverse route with the term $1/k_{mem}$ multiplied by 14, rather than 2, based on our above idealization of seven cell layers in the epithelium.

Paracellular Pathway

Freeze-fracture observations of the epithelium show that tight junctions are localized almost exclusively in the superficial layer, whereas larger gap junctions are found in deeper layers (21). In the absence of specific experimental data regarding the dimensions of the different epithelial junctions, we chose to replace those multiple junctions by one narrow junction, such that the latter would account for the size selectivity imparted by all tight and gap junctions combined. We therefore modeled each intercellular opening as a parallel-wall slit with a narrow section, corresponding to the equivalent junction, followed by a wider one (Fig. 1B). The dimensions of the epithelial narrow junction were chosen so that its effects are equivalent to the combined effects of all epithelial junctions in series, as described below.

Lacking independent data, the large half-width (W_1) was taken to be 15 nm throughout the epithelium, which was based on measurements in endothelium. We estimated the narrow half-width (W_2) based upon the data of Hämäläinen *et al.* (22). In their study, the authors measured the permeability of cornea to small hydrophilic solutes, which diffuse predominantly through the paracellular pathway and for which the epithelium should be by far the tightest barrier. We therefore fitted Eq. 10 to their data; the value of W_2 that yielded the best agreement with experimental observations was 0.8 nm. We further assumed that the length of the equivalent narrow junction in the epithelium was $L_2 = 0.24$ μm, that is, equal to that of endothelial gap junctions. The combined length of the wide channel parts (L_1) was assumed to be equal to the overall distance covered by molecules diffusing alongside the edge of cells minus the length of the tight junction, i.e., $L_{lat} - L_2 = 151.4$ μm.

Given a cell density of $1/(\pi R_i^2)$, the total cell perimeter length per unit area of epithelium, l_c, was calculated as $2/R_i$ (i.e., 1000 cm/cm^2 based on a 20 μm radius for squamous cells; Ref. 15), and f_i was calculated as $W_i \cdot l_c$. With those parameters, the permeability of the paracellular pathway in epithelium was determined using Eqs. 9 and 10.

Whole Cornea

In summary, solute permeability of epithelium and endothelium is each described by the sum of the transcellular

(Eq. 2) and paracellular (Eq. 10) contributions, where different geometric constants (e.g., L_i, L_{lat}, W_i) are used in each tissue, as summarized in Table I. The permeability of stroma is calculated using a fiber-matrix model developed previously (8) and briefly recapitulated in the Appendix. Finally, the overall permeability of the cornea (k_{cornea}) is determined by the series combination of the resistance to transport of the three tissues:

$$\frac{1}{k_{cornea}} = \frac{1}{k_{epi}} + \frac{1}{k_{stroma}} + \frac{1}{k_{endo}} \tag{13}$$

where the subscripts "epi" and "endo" refer to the epithelium and endothelium, respectively.

Calculations for Model Validation and Comparison with Other Theoretical Models

Comparisons between model predictions and experimental data are needed to validate the above model, which we performed using a compilation of experimentally determined permeabilities, as well as distribution coefficients, molecular radii, and other data collected by Prausnitz and Noonan (2). Whole cornea and isolated stroma permeabilities were determined directly through experimentation. However, few direct experimental measurements of corneal endothelial or epithelial solute permeability were made. Instead, literature reports present permeability values for combined layers, such as stroma-plus-endothelium, i.e., de-epithelialized cornea. Indirect experimental values of the permeability of endothelium and epithelium were therefore obtained by considering resistances in series. For example, endothelial permeabilities were determined by subtracting the resistance (i.e., the inverse of the permeability) of stroma from that of stroma-plus-endothelium:

$$\frac{1}{k_{endo}} = \frac{1}{k_{stroma+endo}} - \frac{1}{k_{stroma}} \tag{14}$$

Epithelial permeabilities were calculated in a similar manner, based on reported values for stroma and stroma-plus-epithelium, or for full cornea and de-epithelialized cornea.

These calculations require that the measured values that are combined to yield endothelial or epithelial permeabilities correspond to identical experimental conditions, i.e., same species, temperature, and hydration. We therefore only subtracted resistances when they were reported in the same study. Even in this case, it is, for example, likely that the hydration of stroma was higher when the cell layers were removed, but we did not account for this effect in the absence of specific hydration data. Results for endothelium and epithelium are given in Tables II and III, respectively. In some studies, the measured permeability of several layers combined was higher than that of one layer; such inconsistent data were not included in this analysis.

Uncertainties in these permeability values can be very large, as illustrated by the following example. The reported permeability of stroma to corynanthine is $3.2 \pm 0.6 \times 10^{-5}$ cm/s and that of stroma-plus-endothelium is $3.1 \pm 0.2 \times 10^{-5}$ cm/s (23), yielding a calculated endothelial permeability of $9.9 \pm 78 \times 10^{-4}$ cm/s. Even though experimental standard deviations were small, uncertainty in k_{endo} is much larger than the permeability itself because the two measured values are very close. This constrains our ability to validate model predictions given the large error bars on much of the test data calculated using Eq. 14.

To compare the predictive ability of our model to that of others, we calculated the following sum of squared errors, which is related to a log-scale chi squared (24):

$$SSE = \sum_{i=1}^{n} \left[\frac{\ln(k_{cornea}^{calc})}{\ln(k_{cornea}^{meas})} - 1 \right]^2 \tag{15}$$

where n is the number of solutes considered (e.g., 117 for the cornea) and k_{cornea}^{calc} and k_{cornea}^{meas} are the calculated and measured permeabilities of cornea to solute i, respectively. As an additional characterization, we determined the mean absolute fractional error (MAFE) associated with differences between predicted and measured values, defined as the average absolute value of the residual divided by the actual (i.e., experimental) value (24).

$$MAFE = \frac{1}{n} \sum_{i=1}^{n} \frac{|k_{cornea}^{calc} - k_{cornea}^{meas}|}{k_{cornea}^{meas}} \tag{16}$$

RESULTS AND DISCUSSION

Permeability Predictions

To predict the passive, steady-state permeability of cornea to a broad range of compounds, we developed a theoretical model based on the physicochemical properties of the cornea and diffusing solutes, which were estimated, whenever possible, from independent literature data. Two types of pathways were considered (Fig. 1). Paracellular pathways are water-filled routes between cells in epithelium and endothelium and between the fibers of the largely aqueous stroma. Permeability of these routes is mainly a function of the size and geometry of the pathways and solutes. Transcellular pathways consist of lipid-filled routes within cell membranes. Although the permeability of those pathways also depends upon size and geometry, another important factor is the ability of a solute to partition into cell membranes, as determined by the solute's membrane-to-water distribution coefficient.

Table I. Parameters for Epithelial and Endothelial Permeability Calculations

	Endothelium	Epithelium
Transcellular mean diffusion pathway length (L_{lat})	15.5 μm	151.7 μm
Lateral diffusivity in cell membranes (D_{lat})	2×10^{-8} cm^2/s	2×10^{-8}/cm^2/s
Wide channel half-width (W_1)	15 nm	15 nm
Narrow channel half-width (W_2)	1.5 nm	0.8 nm
Wide channel length (L_1)	12 μm	151.4 μm
Narrow channel length (L_2)	0.24 μm	0.24 μm

Table II. Measured and Calculated Permeabilities of Endothelium[a]

	Measured k_{stroma} (cm/s)	Measured $k_{stroma+endo}$ (cm/s)	Indirectly measured k_{endo} (cm/s)	Predicted k_{endo} (cm/s)	Reference(s)
Acebutolol	3.0E-5	9.3E-6	1.4E-5	1.8E-5	6
Atenolol	3.3E-5	1.6E-5	3.1E-5	7.9E-6	6
Clonidine	4.9E-5	4.7E-5	1.2E-3	1.0E-5	6
Corynanthine	3.2E-5	3.1E-5	9.9E-4	1.2E-3	23
Fluorescein			5.0E-6[c]	6.4E-6	31
Lactate ion			2.8E-5[c]	1.8E-5	31
Mannitol			9.2E-6[c]	1.1E-5	32
Metoprolol	3.4E-5	2.8E-5	1.6E-4	1.0E-5	6
Oxprenolol	3.7E-5	3.1E-5	1.9E-4	2.0E-5	6
Phenylephrine	5.8E-5	2.1E-5	3.3E-5	1.1E-5	23
Phosphate ion			4.4E-6[c]	2.5E-5	33
Propranolol	3.5E-5	3.1E-5	2.7E-4	6.6E-5	6
Rauwolfine	3.6E-5	2.3E-5	6.4E-5	5.9E-5	23
Rubidium ion			3.4E-5[c]	7.2E-5	34
SKF 72 223[b]	4.2E-5	3.9E-5	4.9E-4	1.9E-5	23
SKF 86 466[b]	5.7E-5	5.3E-5	8.4E-4	2.6E-4	23
Sucrose			5.9E-6[c]	7.3E-6	32,35,36
Thiocyanate ion			2.5E-5[c]	2.5E-5	34
Urea			2.0E-5[c]	2.1E-5	35,36

[a] As discussed in the "Model Development" section, experimental permeability measurements were obtained from the references listed and treated mathematically using Eq. 14.
[b] SKF 72 223: 5,8 Dimethoxy-1,2,3,4-tetrahydroisoquinoline; SKF 86 466; 6-Chloro-3-methyl-2,3,4,5-tetrahydro-1H-3-benzazepine.
[c] Measured directly.

Figure 2A shows the predicted permeability as a function of solute radius and distribution coefficient in each of the cornea's three primary layers: endothelium, stroma, and epithelium. Results are given for solutes ranging from 3.5 to 5.5 Å in radius (i.e., about 100 to 500 Da molecular weight); macromolecules are too large to diffuse across cornea and are therefore not included. Figure 2A suggests that the permeability of stroma, a water-filled fibrous medium composed mostly of collagen and glycosaminoglycans, depends only on solute radius (r_s) and not on distribution coefficient (Φ) because there is no favored pathway for hydrophobic compounds (because Φ is a measure of partitioning between water and lipid, it does not influence partitioning between water and stroma). In the endothelium and epithelium, the permeability increases with both decreasing solute radius and increasing solute distribution coefficient.

When distribution coefficients are small, solutes diffuse predominantly through the paracellular routes around cells so that endothelial and epithelial permeabilities are a function of size only. As Φ increases from approximately 0.01 to 10, the contribution of the transcelullar pathways becomes progressively more important, and permeabilities rise with the distribution coefficient. This increase is all the more pronounced for the larger solutes because they have a lower paracellular permeability as a result of hindered transport through tight and gap junctions. For values of Φ greater than 10, the transcellular route is dominant, and the permeability of the cell layers becomes mainly a function of distribution coefficient.

Permeability predictions for the entire cornea are shown in Fig. 2B. Using the equations developed above, model predictions can be made for any compound of known radius and distribution coefficient. For small Φ values, the permeability is essentially a function of solute size, since only hydrophilic pathways are accessible. Comparison with Fig. 2A shows that for such solutes, the epithelium is by far the main barrier to diffusion, with permeabilities that are more than an order of magnitude smaller than those of the endothelium and about two orders of magnitude smaller than those of stroma. Diffusing across the paracellular route of the epithelial layer is thus the rate-limiting step, and the permeability is governed by size.

As Φ increases from 0.01 to 10, the epithelial layer is still the most restrictive, but the transcellular pathway becomes more and more important as the hydrophobic routes become increasingly accessible. Thus, the permeability becomes increasingly a function of distribution coefficient, and differences between solutes of varying sizes are attenuated. This is expected because we assumed that the value of lateral diffusivity in endothelial and epithelial cells is constant (i.e., independent of solute radius), which is a justifiable hypothesis given that the size range of the compounds considered here is small ($3.5\ \text{Å} \leq r_s \leq 5.5\ \text{Å}$).

For Φ greater than 10, the transcellular routes through the endothelium and epithelium are less and less restrictive and the stroma becomes the main barrier; hence, the increased dependence of the overall permeability on solute radius. It should be noted that the endothelium is never the rate-limiting barrier for diffusion across the whole cornea.

It is important to note that these equations predict permeability and not flux across the corneal tissues. Permeability is an intrinsic measure of how easily a molecule can diffuse across a tissue, which is independent of apparatus and protocol. However, the diffusive flux (J) of a molecule is a protocol-dependent quantity that is determined by both the tissue permeability (k) and the concentration difference of the molecule across the tissue (ΔC):

$$J = k\,\Delta C \tag{17}$$

Table III. Measured and Calculated Permeabilities of Epithelium[a]

	Measured k_{cornea} (cm/s)	Measured $k_{endo+stroma}$ (cm/s)	Indirectly measured k_{epi} (cm/s)	Predicted k_{epi} (cm/s)	Reference(s)
Acebutolol	8.5E-7	9.3E-6	9.4E-7	1.7E-6	6
Acetazolamide	5.1E-7	9.7E-6	5.4E-7	9.8E-7	37
Acetazolamide der. 1[b]	6.0E-7	8.3E-6	6.5E-7	1.3E-6	37
Acetazolamide der. 2[b]	5.6E-7	9.7E-6	5.9E-7	1.2E-6	37
Alpha-Yohimbine	2.3E-5	3.8E-5	5.9E-5	9.8E-5	23
Atenolol	6.8E-7	1.6E-5	7.1E-7	6.4E-7	6
Benzolamide	1.4E-7	1.1E-5	1.4E-7	7.7E-7	38
Bromacetazolamide	3.6E-7–4.0E-7	8.7E-6–9.7E- 6	4.0E-7	8.3E-7	37,39
Chlorzolamide	1.8E-5	3.6E-5	3.6E-5	2.7E-5	37
Clonidine	3.1E-5	4.7E-5	8.8E-5	8.2E-7	23
Corynanthine	1.1E-5	3.1E-5	1.8E-5	1.2E-4	23
Levobunolol	1.7E-5	2.5E-5	5.3E-5	4.6E-6	6
Methazolamide	2.6E-6–4.9E-6	1.8E-5–2.2E- 5	4.7E-6	8.7E-7	37,38
Methazolamide der.[c]	7.8E-7	1.7E-5	8.2E-7	9.6E-7	37
Metoprolol	2.4E-5	2.8E-5	1.7E-4	8.6E-7	6
Nadolol	1.6E-6	1.5E-5	1.8E-6	5.9E-7	6
Oxprenolol	2.6E-5[d]	3.7E-5[d]	8.8E-5	1.9E-6	6
Phenylephrine	9.4E-7	2.1E-5	9.8E-7	8.7E-7	23
Rauwolfine	9.2E-6	2.3E-5	1.5E-5	5.9E-6	23
Sotalol	1.0E-6	1.8E-5	1.0E-6	6.5E-7	6
Timolol	1.2E-5	2.6E-5	2.2E-5	2.2E-6	6
Trichlormethazolamide	1.0E-5–1.1E-5	3.7E-5–3.9E- 5	1.5E-5	2.1E-6	37,39
Trifluormethazolamide	3.9E-6	1.8E-5	5.0E-6	9.5E-7	37
Vidarabine	1.7E-6	1.6E-5	1.9E-6	7.1E-7	40
Yohimbine	1.8E-5	3.7E-5	3.7E-5	8.9E-5	23

[a] As discussed in the "Model Development" section, experimental permeability measurements were obtained from the references listed and treated mathematically using Eq. 14.
[b] Acetazolamide derivatives: 2-Benzoylamino-1,3,4-thiadiazole 5-sulfonamide (1); 2-Isopentenyl amino 1,3,4-thiadiazole-5-sulfonamide (2).
[c] Methazolamide derivative: 5-Imino-4-methyl-1,3,4 thiadiazoline-2-sulfonamide.
[d] The first and second numbers given for oxprenolol correspond to its permeability in stroma-plus-epithelium and in stroma only, respectively.

Thus, the model correctly predicts that corneal permeability increases (and then plateaus) with decreasing hydrophilicity (Fig. 2B). However, as Φ increases, the peak flux is expected to increase, go through a maximum and then decrease due to competing effects of permeability rising and aqueous (i.e., tear film) solubility diminishing for more hydrophobic compounds.

It is also important to note that the permeability calculated here describes the ability of molecules to traverse the cornea at steady state. Typically, there is a transient period during which flux increases from zero to its steady state value, e.g., after administration of eye drops. Only during steady state is the flux constant both in time and space and given by Eq. 17; during the transient period, solute flux should scale with permeability (in the absence of binding or other complicating factors) but will result in less transport than during steady state, as described in our study of transient transport in sclera (25).

Model Validation

Comparisons between experimental data and model predictions for the endothelium, epithelium, and full cornea are shown in Fig. 3. If the match were perfect, all data points would fall on the diagonal on each graph. In each case, model predictions are almost all within a factor 10 of experimental data. There is no consistent over- or underprediction, suggesting that there is no systematic error in the model. As discussed in the "Model Development" section and below, in many cases the accuracy of experimental data is only plus-or-minus a factor 10, meaning that the model predictions are generally within the range of experimental certainty. Order-of-magnitude predictive ability may not be sufficient in some cases, but as an easily determined first estimate and guide, this level of broad predictive ability should be useful.

In the endothelium (Fig. 3A) and epithelium (Fig. 3B), agreement between predicted and indirectly measured (Tables II and III) permeability values is quite good, given the simplifying assumptions made in the model. In endothelium, predicted and measured permeabilities are within a factor 10 of each other in 16 of 19 cases and have an overall MAFE = 0.74. In the epithelium, predicted and measured permeabilities are within a factor 10 of each other in 20 of 25 cases, with MAFE = 1.07. Moreover, if we consider only those solutes for which the permeability was measured directly, the agreement is even better (Tables II and III). Uncertainties in the "indirectly" measured values, which can be very large as discussed above, may well be the source of the few large discrepancies that are observed. For example, the standard deviation associated with the indirectly "measured" endothelial permeability value for clonidine and SKF 72 223 is as much as 250% and 80%, respectively. Model predictions for stromal permeability were similarly validated in our previous paper (8).

Combining all these data, measured (from Ref. 2) and calculated permeabilities for the whole cornea are plotted in

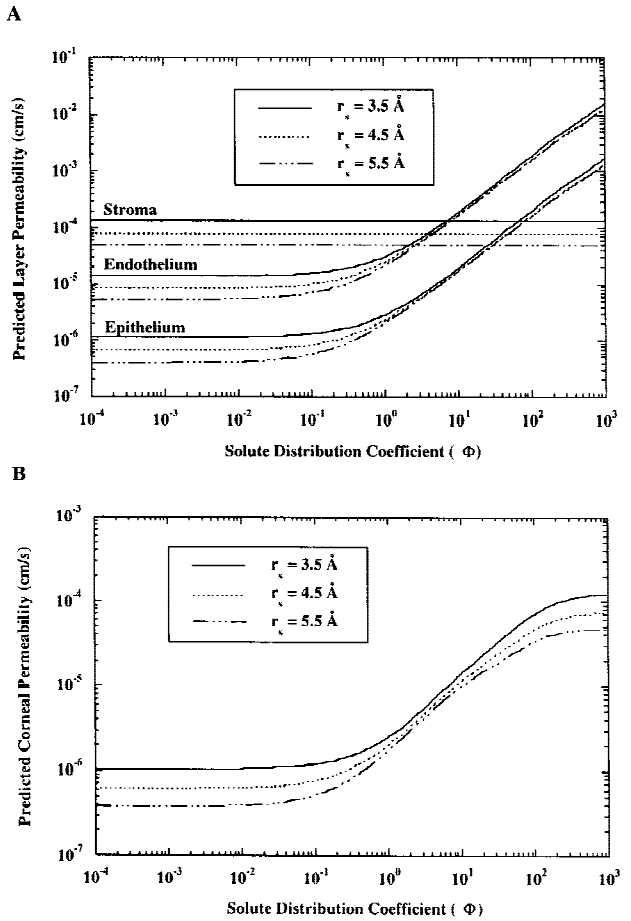

Fig. 2. Predicted permeability versus solute distribution coefficient for different values of solute size shown: (A) in the corneal epithelium (Eq. 1), stroma (Eq. A1), and endothelium (Eq. 1) and (B) in the whole cornea (Eq. 13). As discussed in the text, transport of hydrophilic compounds is limited primarily by the epithelial barrier, whereas very hydrophobic compounds are limited primarily by the stroma. For reference, the range of solute radii (3.5–5.5 Å) encompasses a molecular weight range of approximately 100–500 Da.

Fig. 3C. The agreement between measured and predicted values is generally good; there is less than a factor 10 difference for 110 of 117 solutes and MAFE = 2.43. As evidenced by the scatter in the data, there are a few instances in which the measured permeability of two solutes with similar radii and similar distribution coefficients differs by more than a factor 100. The present model, because it predicts permeability as a function of size and hydrophilicity, cannot account for such variations, which could stem from differences in solute properties that the model does not take into consideration (e.g., shape, dipole interaction), but are more likely due to experimental variations and/or uncertainties, as discussed above.

Comparison with Other Theoretical Models

Other approaches have been developed to predict the permeability of cornea and have reached many of the same qualitative conclusions as the present work. In the model of Grass *et al.* (4), which extends the analysis of Cooper and Kasting (3), the cornea was represented as a laminated membrane with a lipid layer (epithelium) and an aqueous layer (stroma), and with aqueous pores present in the epithelium. Constants related to the apparent diffusion coefficients for the stroma, the lipid epithelium and the epithelial pores were obtained by data fitting. The model presented by Huang *et al.* (6) also represented cornea as a laminate membrane with three distinct layers: epithelium, stroma, and the endothelium. Using their experimental data and an equation similar to our Eq. 3, they developed an expression for corneal permeability based partly on geometric measurements and partly on fitting their data. Worth and Cronin (7) developed an empirical correlation based on physicochemical properties of solutes and non-linear regression of the data set assembled by Prausnitz and Noonan (2).

Shown in Table IV are the values of sum of squared errors (SSE) and MAFE obtained by comparing experimental and predicted permeability values for the set of solutes given in reference (2) using our model and that of others (3,4,6,7). As illustrated, the predictive ability of the model presented here is significantly better than that of three of the four previous approaches examined (3,4,6). It is not surprising that the correlation developed by Worth and Cronin (7) yields smaller SSE and MAFE values than ours because its parameters were obtained by fitting this entire set of data. Although a few parameters in our model (e.g., D_{lat}, k^0_{mem}, W_2 in epithelium) were determined by fitting independent data, the model itself was not fitted to any given set of permeability measurements; the independent data used to estimate unknown parameters were not included in the set with which our predictions were ultimately compared, as opposed to what was done in all four other modeling studies (3,4,6,7).

We believe that the strength of our approach lies in the fact that every parameter is related to the actual physical structures that make up cornea, that all parameter values are estimated using different, independent sources of data, and that the model is therefore more broadly applicable. The model of Yoshida and Topliss (5) is not included in this comparison, because it requires alkane-to-water partition coefficients, which we were unable to obtain.

Implications for Drug Delivery

This model for corneal permeability should be useful for drug delivery because it provides a relatively simple method to calculate corneal permeability to any compound. Although experiments ultimately will be needed for any promising new drug, initial estimates of corneal permeability can be made knowing only the following two parameters: 1) molecular radius, which can be determined using established correlations based on molecular weight and/or chemical structure (19) and 2) octanol–water distribution coefficient, which can be measured experimentally or calculated using semi-empirical correlations for octanol–water partition coefficient (26) and degree of ionization (27).

Model predictions can help develop drug delivery strategies. Figure 4A identifies the predicted rate-limiting pathway as a function of solute distribution coefficient for solutes of two different representative sizes. For compounds with a distribution coefficient less than about 0.1 or 1 (depending on solute size), the rate-limiting layer for transcorneal transport is epithelium and the available pathway within the epithelium is the paracellular route. For compounds having intermediate distribution coefficients, permeability is primarily determined by the transcellular route across epithelium. Compounds with

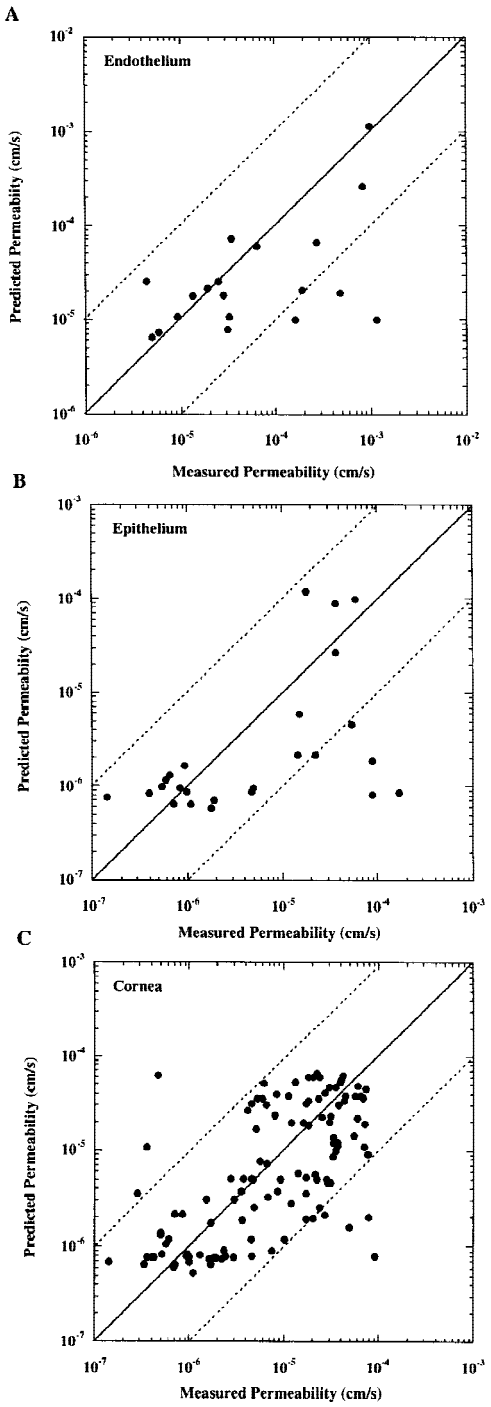

Fig. 3. Validation of model permeability predictions by comparison with experimental values for compounds believed to passively diffuse across ocular tissues: (A) endothelium (sum of squared errors, SSE = 5.02×10^{-2}; mean absolute fractional error, MAFE = 0.74; data from Table II; prediction using Eq. 1), (B) epithelium (SSE = 4.00×10^{-2}; MAFE = 1.07; data from Table III; prediction using Eq. 1), and (C) whole cornea (SSE = 1.52×10^{-2}; MAFE = 2.43; measured permeabilities from Ref. 2; prediction using Eq. 13). Almost all predicted permeabilities agree with experimental measurements with an accuracy of at least a factor 10 (indicated by the dotted lines). As explained in the text, the uncertainty associated with many of the experimental measurements can be plus-or-minus a factor 10, meaning that order-of-magnitude agreement is generally the best possible validation using the available data collected by many different labs under somewhat different conditions.

distribution coefficients larger than about 10 or 100 (again, depending on solute size) are rate limited by the stroma. This means that strategies to enhance corneal permeabilities should focus primarily on the paracellular or transcellular route across epithelium and possibly on stroma.

Even though our model is based upon an idealized representation of the corneal ultrastructure, its parameters are all related to physical observations and measurements. This model can therefore be extended to compounds not considered in the analysis used to validate it because it predicts corneal permeability for any compound for which size and distribution coefficient are known. This could be especially useful to drug designers to estimate corneal permeability to newly designed or synthesized compounds. Because the model also allows one to vary physicochemical properties of corneal tissue, it can be used to predict permeability of, for instance, diseased cornea with altered microanatomy and/or chemical content. It could also facilitate predictions of corneal permeability at different stages of pediatric and possibly neonatal development, as well as predictions in animals.

To identify effects of changing physicochemical properties on corneal permeability, in Fig. 4 we then performed a sensitivity analysis by assessing the effects on whole cornea permeability caused by doubling the value of each of the main parameters. As illustrated in Fig. 4B, epithelial permeability to very hydrophilic solutes (black bars) is affected strongly by the width and length of intercellular spaces (i.e., L_i and W_i), consistent with solutes following paracellular pathways. In contrast, very hydrophobic compounds (gray bars) are relatively unaffected by any of the parameters shown, because their transport is limited by stroma. Finally, an intermediate compound expected to primarily follow a transcellular route shows strong dependence on the length L_1 and diffusivity D_{lat} characterizing the transcellular lateral pathway. The effects on endothelium are similarly considered in Fig. 4C. Because the endothelium is never a rate-limiting barrier, changes in endothelial parameters have almost no effect on corneal permeability to any of the solutes considered.

We also examined the effects caused by changes in stromal parameters (the meaning of these parameters is presented and discussed in our previous paper (8), where the model for stroma was developed). Stromal parameters do not affect the corneal permeability to hydrophilic solutes, as shown in Fig. 4D, because the stroma is the rate-limiting barrier only for hydrophobic solutes. For hydrophobic solutes, a factor two increase in the solid volume fraction occupied by glycosaminoglycans or by core proteins (both of which form the ground substance) results in a significant permeability reduction. Conversely, permeability increases with the core protein radius when solid volume fractions are kept constant, since the spaces between the fibers are then larger. As expected, doubling stromal thickness lowers corneal permeability by almost half. Finally, when stromal hydration is increased from 78% to 86% (the value we used in the denuded stroma studies), solid volume fractions in stroma are smaller, rendering the layer much more permeable; the corneal permeability of a very hydrophobic solute then increases by about 15%.

Limitations of the Model

It was possible to validate this model only with order-of-magnitude certainty, given the broad range of corneal perme-

Table IV. Comparison of Predictive Ability of Corneal Permeability Models

Model	Sum of squared errors[a]	Mean absolute fractional error[a]	Reference
Edwards and Prausnitz	1.52E-2	2.43	This work
Worth and Cronin	1.31E-2	1.04	7
Huang *et al.*	1.52E-2	4.49	6
Grass *et al.*	4.40E-2	28.86	4
Cooper and Kastings	7.76E-2	28.18	3

[a] Predictions of corneal permeability were made using each model and compared to 117 experimental data points tabulated in Ref. 2. The "Model Development" section contains definitions of the statistical terms.

abilities reported in different studies for the same molecules or for molecules with similar physicochemical properties (2) and the large uncertainly associated with permeabilities indirectly measured for isolated epithelium and endothelium (Tables II and III). However, for initial estimates of corneal permeability to guide subsequent experiments, order of magnitude certainty may often be sufficient.

Several intrinsic limitations of this model need to be acknowledged. Firstly, our representation of intercellular openings and tight junctions in epithelium and endothelium, which

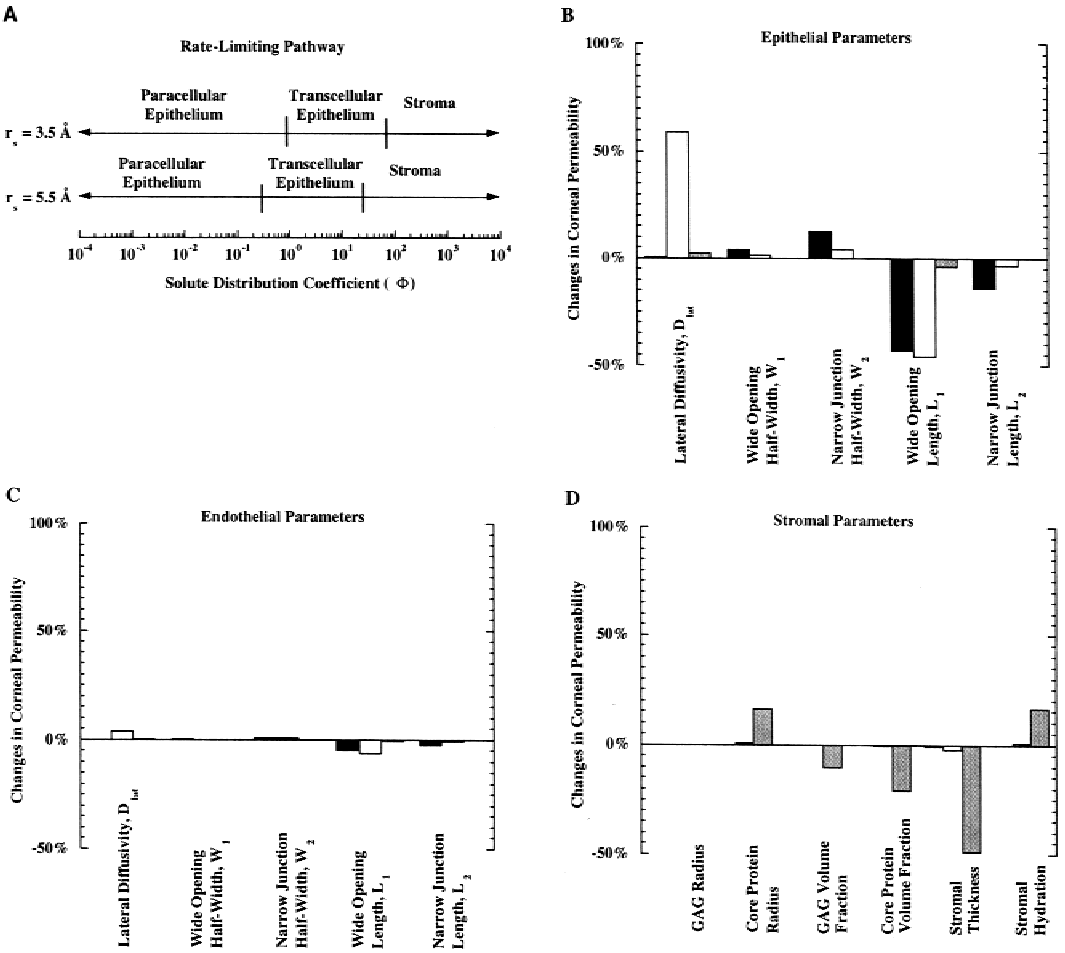

Fig. 4. Influence of physical properties of the eye and solutes on corneal permeability. (A) Predicted rate-limiting barrier as a function of solute distribution coefficient, for two representative solute sizes. As distribution coefficient increases, the primary barrier shifts progressively from paracellular paths across the epithelium to transcellular paths across epithelium to stroma. Effects on corneal permeability caused by changes in the ultrastructural parameters that characterize the (B) epithelium (Eq. 1), (C) endothelium (Eq. 1), and (D) stroma (Eq. A1). Three representative solutes are chosen, all of radius 5 Å; the octanol-to-water distribution coefficient of the hydrophilic compound is 1×10^{-3} (black bars), that of the intermediate compound is 1×10^{0} (white bars), and that of the hydrophobic one is $1 \times 10^{+3}$ (gray bars). All ultrastructural parameters were increased by a factor 2 (except for stromal hydration, which is increased from 78% to 86%; see text). For baseline values for epithelium and endothelium, see Table I; for stroma, see Ref. 8.

are in reality complex and difficult to model, is much simplified. Moreover, epithelial cells are asymmetric, with the apical and basolateral surfaces exhibiting different membrane morphology and ionic permeabilities (10). There is also evidence that different epithelial cell layers have different permeability characteristics. In our approach, however, the lateral diffusivity in the cell membrane is taken to be constant throughout the epithelium, and such differences are not taken into consideration. Possible binding of solutes within the cornea was also not addressed, lacking knowledge of which molecules would bind and the corresponding binding kinetics, number of binding sites, etc.

In the absence of cell membrane permeability data for larger molecules, we had to extrapolate data obtained for solutes with a molecular volume lower than 73 cm^3/mol, and it is possible that we may have incorrectly estimated the contribution of the transverse pathway directly across cells. Finally, as discussed above, the model does not account for differences in solute shape, but assumes that all compounds can be approximated as solid spheres.

CONCLUSION

Using a composite porous-medium analysis of epithelium and endothelium and a fiber-matrix analysis of stroma, we developed an ultrastructural model to predict corneal permeability to drugs and other solutes, based upon physical measurements. The model was validated by comparison with more than 150 experimental data points. In addition, by determining the relative contribution of paracellular and transcellular routes within each corneal sub-layer (i.e., epithelium, stroma and endothelium), we identified the rate-limiting pathways to target for enhancement as a function of solute size and hydrophilicity. We also studied the general effects of changing physical properties on corneal permeability.

ACKNOWLEDGMENTS

We thank Drs. Mark Johnson, Samir Mitragotri, William Deen, Henry Edelhauser, and Dayle Geroski for helpful discussions. This work was supported in part by the National Science Foundation.

APPENDIX

Determination of Stromal Permeability

Calculations to determine the permeability of stroma were described in detail in our earlier work (8) and summarized below. The permeability of stroma (k_{stroma}) to a given solute is

$$k_{stroma} = \frac{D^{eff}}{L_{stroma}} \tag{A1}$$

where the effective diffusivity, D^{eff}, is the product of the solute partition coefficient and solute diffusivity in stroma, and L_{stroma} is the thickness of the membrane, taken to be 0.45 mm.

We distinguish three length scales in stroma: at the macroscale, collagen lamellae form sheets that are taken to be parallel to the anterior surface; at the mesoscale, collagen fibrils within the lamellae constitute hexagonal arrays; and at the microscale, the ground substance consists of a randomly-oriented collection of fibers, representing the proteoglycans.

The microscale effective diffusivity in the ground substance (D_{gs}^{eff}) must be determined first and is given by (28,29):

$$D_{gs}^{eff} = D_\infty \frac{\exp(-f^2)\exp(-0.84f^{1.09})}{1 + \frac{r_s}{\sqrt{K_{gs}}} + \frac{(r_s/\sqrt{K_{gs}})^2}{3}} \tag{A2}$$

$$f = 0.021(1 + r_s/r_f)^2$$

where r_f = 0.39 nm is the average radius of fibers in the ground substance, K_{gs} = 2.9 nm^2 is the Darcy (hydrostatic) permeability of the ground substance, f is the adjusted volume fraction of fibers, and electrostatic interactions are neglected.

The mesoscale effective diffusivity in the collagen lamellae (D_{lam}^{eff}) is then calculated as:

$$\frac{D_{lam}^{eff}}{D_{gs}^{eff}} = 1 - 2\phi_{cf}\left(1 + \phi_{cf} - \frac{C_1\phi_{cf}^{\,6}}{1 - C_2\phi_{cf}^{\,12}} - C_3\phi_{cf}^{\,12}\right)^{-1} \tag{A3}$$

$$\phi_{cf} = 0.27(1 + r_s/r_{cf})^2$$

where r_{cf} = 15 nm is the average radius of the collagen fibrils in the lamellae, and C_1 = 0.075422, C_2 = 1.060283, C_3 = 0.000076 are given constants (30).

At the macroscale, we need to replace our previous description of the collagen lamellae as a periodic array of cylinders (8) with a more accurate representation in which they form thin, parallel sheets (10). The numerical predictions that result from this change differ by approximately 15% from previous calculations (data not shown). Given this geometry, the effective diffusivity at the macroscale is equal to that at the mesoscale, i.e., $D^{eff} = D_{lam}^{eff}$, and the permeability to stroma is calculated using Equation A1.

REFERENCES

1. W. Tasman (ed.). *Duane's Foundations of Clinical Ophthalmology*, Lippincott-Raven, Philadelphia, 1995.
2. M. R. Prausnitz and J. Noonan. Permeability of cornea, sclera, and conjunctiva: a literature analysis for drug delivery to the eye. *J. Pharm. Sci.* **87**:1479–1488 (1998).
3. E. R. Cooper and G. Kasting. Transport across epithelial membranes. *J. Control. Release* **6**:23–35 (1987).
4. G. M. Grass, E. R. Cooper, and J. R. Robinson. Mechanisms of corneal drug penetration. III. Modeling of molecular transport. *J. Pharm. Sci.* **77**:24–26 (1988).
5. F. Yoshida and J. G. Topliss. Unified model for the corneal permeability of related and diverse compounds with respect to their physicochemical properties. *J. Pharm. Sci.* **85**:819–823 (1996).
6. H.-S. Huang, R. D. Schoenwald, and J. L. Lach. Corneal penetration behavior of beta-blocking agents II: Assessment of barrier contributions. *J. Pharm. Sci.* **72**:1272–1279 (1983).
7. A. P. Worth and M. T. D. Cronin. Structure-permeability relationships for transcorneal penetration. *ATLA* **28**:403–413 (2000).
8. A. Edwards and M. R. Prausnitz. A fiber matrix model for the permeability of sclera and corneal stroma. *AIChE J.* **44**:214–225 (1998).
9. D. M. Maurice. The permeability of the cornea. *Ophthal. Lit.* **7**:3–26 (1953).
10. I. Fatt and B. A. Weissman. *Physiology of the Eye. An Introduction to the Vegetative Functions*, 2nd ed., Butterworth-Heinemann, Boston, 1992.
11. M. Johnson, D. Berk, D. Blankschtein, D. Golan, R. Jain, and R. Langer. Lateral diffusion of small compounds in human stratum

corneum and model lipid bilayer systems. *Biophys. J.* **71**:2656–2668 (1996).
12. P. R. Dragsten, R. Blumenthal, and J. S. Handler. Membrane asymmetry in epithelia: Is the tight junction a barrier to diffusion in the plasma membrane? *Nature* **294**:718–722 (1981).
13. J. Fischbarg. Active and passive properties of the rabbit corneal endothelium. *Exp. Eye Res.* **15**:615–638 (1973).
14. W. R. Lieb and W. D. Stein. Non-stokesian nature of transverse diffusion within human red cell membranes. *J. Membr. Biol.* **92**: 111–119 (1986).
15. H. P. Kao, J. R. Abney, and A. S. Verkman. Determinants of the translational mobility of a small solute in cell cytoplasm. *J. Cell Biol.* **120**:175184 (1993).
16. J. Brunner, D. E. Graham. H. Hauser, and G. Semenza. Ion and sugar permeabilities of lecithin bilayers: comparison of curved and planar bilayers. *J. Membr. Biol.* **57**:133–141 (1980).
17. M. A. Akeson and D. N. Munns. Lipid bilayer permeation by neutral aluminum citrate and by three α–hydroxy carboxylic acids. *Biochim. Biophys. Acta* **984**:200–206 (1989).
18. Y. Panwar and J. L. Anderson. Hindered diffusion in slit pores: an analytical result. *Ind. Eng. Chem. Res.* **32**:743–746 (1993).
19. B. E. Poling, J. M. Prausnitz, and J. P. O'Connell. *The Properties of Gases and Liquids*, 5th ed., McGraw-Hill, New York, 2000.
20. D. M. Maurice. Passive ion fluxes across the corneal endothelium. *Curr. Eye Res.* **4**:339—349 (1985).
21. M. Tanaka, Y. Ohnishi, and T. Kuwabara. Membrane structure of corneal epithelium: freeze-fracture observation. *Jpn. J. Ophthalmol.* **27**:434–443 (1983).
22. K. M. Hämäläinen, K. Kontturi, S. Auriola, L. Murtomäki, and A. Urtti. Estimation of pore size and pore density from permeability measurements of polyethylene glycols using an effusion-like approach. *J. Control. Release* **49**:97–104 (1997).
23. C.-H. Chiang, R. D. Schoenwald, and H.-S. Huang. Corneal permeability of adrenergic agents potentially useful in glaucoma. *J. Taiwan Pharm. Assoc.* **38**:67–84 (1986).
24. J. L. Devore. *Probability and Statistics for Engineering and the Sciences*, 4th ed., Duxbury Press, Belmont, 1995.
25. M. R. Prausnitz, A. Edwards, J. S. Noonan, D. E. Rudnick, H. F. Edelhauser, and D. H. Geroski. Measurement and prediction of transient transport across sclera for drug delivery to the eye. *Ind. Eng. Chem. Res.* **37**:2903–2907 (1998).
26. A. Albert and E. P. Serjeant. *The Determination of Ionization Constants*, Chapman and Hall, London, 1984.
27. W. J. Dunn, J. H. Block, and R. S. Pearlman (eds.), *Partition Coefficient Determination and Estimation,* Pergamon Press, New York, 1986 pp. 3–20.
28. D. S. Clague and R. J. Phillips. Hindered diffusion of spherical macromolecules through dilute fibrous media. *Phys. Fluids* **8**: 1720–1731 (1996).
29. E. M. Johnson, D. A. Berk, R. K. Jain, and W. M. Deen. Hindered diffusion in agarose gels: test of effective medium model. *Biophys. J.* **70**:1017–1026 (1996).
30. W. T. Perrins, D. R. McKenzie, and R. C. McPhedran. Transport properties of regular arrays of cylinders. *Proc. R. Soc. Lond. A* **369**:207–225 (1979).
31. P. N. Hale and D. M. Maurice. Sugar transport across the corneal endothelium. *Exp. Eye Res.* **8**:205–215 (1969).
32. J. H. Kim, K. Green, M. Martinez, and D. Paton. Solute permeability of the corneal endothelium and Descemet's membrane. *Exp. Eye Res.* **12**:231–238 (1971).
33. S. Hodson and F. Miller. The bicarbonate ion pump in the endothelium which regulates the hydration of rabbit cornea. *J. Physiol.* **263**:563–577 (1976).
34. D. M. Maurice. The cornea and sclera. In H. Davidson (ed.), *The Eye: Vegatative Physiology and Biochemistry,* Academic Press, Orlando, Florida, 1984 pp. 1–129.
35. M. V. Riley. A study of the transfer of amino acids across the endothelium of the rabbit cornea. *Exp. Eye Res.* **24**:35–44 (1977).
36. S. Mishima and S. M. Trenberth. Permeability of the corneal endothelium to nonelectrolytes. *Invest. Ophthalmol.* **7**:34–43 (1968).
37. T. H. Maren, L. Jankowska, G. Sanyal, and H. F. Edelhauser. The transcorneal permeability of sulfanomide carbonic anhydrase inhibitors and their effect on aqueous humor secretion. *Exp. Eye Res.* **36**:457–480 (1983).
38. H. F. Edelhauser and T. H. Maren. Permeability of human cornea and sclera to sulfonamide carbonic anhydrase inhibitors. *Arch. Ophthalmol.* **106**:1110–1115 (1988).
39. L. Jankowska, A. Bar-Ilan, and T. Maren. The relations between ionic and non-ionic diffusion of sulfonamides across the rabbit cornea. *Invest. Ophthal. Vis. Sci.* **27**:29–37 (1986).
40. W. J. O'Brien and H. F. Edelhauser. The corneal penetration of trifluorothymidine, adenine arabinoside, and idoxuridine: a comparative study. *Invest. Ophthal. Vis. Sci.* **16**:1093–1103 (1977).